RESEARCH ARTICLE

NANO · MICRO small
www.small-journal.com

Long-Distance Charge Transport between Cytochrome *c* and Complex III is Mediated by Protons and Reactive Oxygen Species

*Anna Lagunas, Alexandre M. J. Gomila, Alba Nin-Hill, Alejandra Guerra-Castellano, Gonzalo Pérez-Mejías, Josep Samitier, Carme Rovira, Miguel A. De la Rosa, Irene Díaz-Moreno, and Pau Gorostiza**

Electron transfer (ET) between redox proteins is an essential process in the respiratory and photosynthetic transport chains. While intra-protein ET is well characterized, the experimental methods to investigate inter-protein ET are limited by the presence of the solvent and by the transient nature of the protein–protein interaction and ET event, which are averaged in protein ensembles. Wiring precisely oriented redox protein partners to the nanoscale electrodes of an electrochemical scanning tunneling microscope allows recording the time- and distance-dependence of the current flowing between them. These methods have revealed that the current flowing between individual protein pairs extends beyond tunneling distances and that it is electrochemically gated. However, the corresponding mechanism and the identity of the charge carriers in aqueous solution remain to be elucidated. To determine the species involved in long-distance charge transport between the redox partner proteins C*c* and Cc_1 of the respiratory chain, recordings are performed as a function of pH, in heavy water solutions, and in degassed solutions. It is observed that the spatial span and electrochemical gating of long-distance currents are reduced at high pH, in heavy water, and at low oxygen concentration, showing that the currents are assisted by superoxide anions and by protons.

1. Introduction

Charge transport in biological systems involves consecutive electron transfer (ET) events through redox proteins, resulting in a tightly regulated flow of electrons. These processes are essential for the respiratory and photosynthetic electron transport chains that sustain life.

Intra-protein ET between redox sites at fixed positions within the protein is well studied and has been characterized by cyclic voltammetry on metal electrodes, laser flash photolysis with covalently conjugated photoinduced redox labels, transient optical absorption studies, or nuclear magnetic resonance spectroscopy. Experimental and theoretical methods have shown that intra-protein ET between redox sites within a protein complex (e.g., between c_1 and FeS sites in the respiratory complex III, i.e., cytochrome bc_1, Figure S1a, Supporting Information) proceeds by a

A. Lagunas, A. M. J. Gomila[+], J. Samitier, P. Gorostiza
Biomaterials, and Nanomedicine (CIBER-BBN)
CIBER-BBN, ISCIII
Madrid 28029, Spain
E-mail: pau@icrea.cat

The ORCID identification number(s) for the author(s) of this article can be found under https://doi.org/10.1002/smll.202501286

[+]Present address: Jülich Research Center, 52428 Jülich, Germany

[++]Present address: Toulouse Biotechnology Institute, Université de Toulouse, CNRS, INRAE, INSA, Toulouse Cedex F-31077, France

DOI: 10.1002/smll.202501286

A. Lagunas, J. Samitier
Nanobioengineering Group, Institute for Bioengineering of Catalonia (IBEC)
The Barcelona Institute for Science and Technology (BIST)
Barcelona 08028, Spain

A. M. J. Gomila[+], P. Gorostiza
Nanoprobes and Nanoswitches Group, Institute for Bioengineering of Catalonia (IBEC)
The Barcelona Institute for Science and Technology (BIST)
Barcelona 08028, Spain

A. Nin-Hill[++], C. Rovira
Department of Inorganic and Organic Chemistry (Orgaic Chemistry Section) & Institute of Theoretical and Computational Chemistry (IQTCUB)
University of Barcelona
Barcelona 08028, Spain

A. Guerra-Castellano, G. Pérez-Mejías, M. A. D. la Rosa, I. Díaz-Moreno
Institute for Chemical Research–cicCartuja, Universidad de Sevilla
Consejo Superior de Investigaciones Científicas (CSIC)
Sevilla 41092, Spain

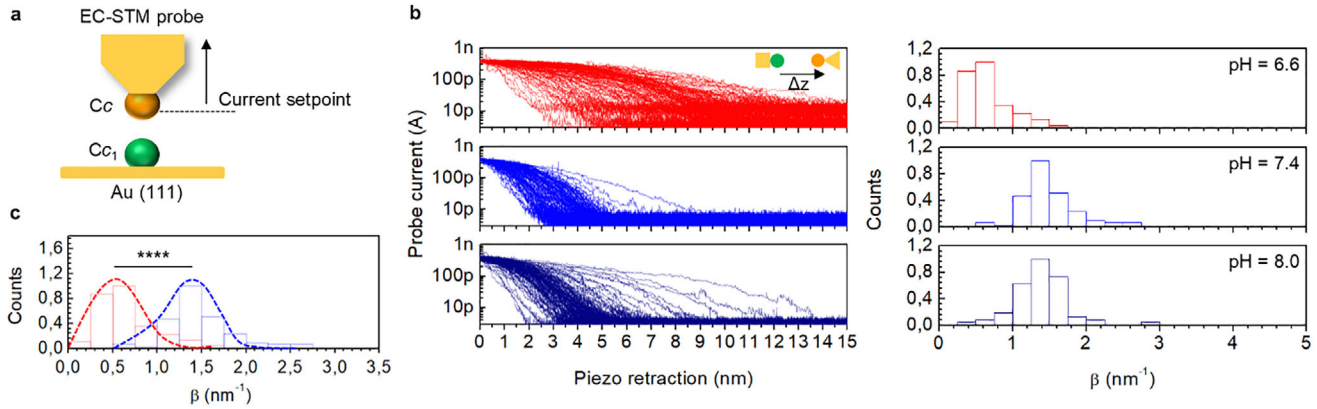

Figure 1. Effect of proton concentration in the current-distance decay between Cc_1-Cc. a) Scheme of the current-distance (I-z) measurement between Cc and Cc_1 with EC-STM showing Cc (orange) bound to the EC-STM probe and Cc_1 (green) bound to the surface of Au(111) electrode. b) Ensemble of semi-logarithmic I-z curves (left) obtained in 50 mM phosphate buffer at pH 6.6 (red), pH 7.4 (blue), and pH 8.0 (purple), and the corresponding histograms of distance decay factors (β) quantified from individual curves (right). c) Comparison of the averaged β values for Cc-Cc_1, $\beta = 0.6 \pm 0.3$ nm^{-1} at pH = 6.6 (n = 123 curves, N = 2, red) and $\beta = 1.5 \pm 0.4$ nm^{-1} at pH = 7.4 (n = 109 curves, N = 2, blue), respectively, showing significant differences (Mann Whitney test, U = 748, two-tailed, ****$p < 0.0001$).

combination of electron tunneling steps and conduction through covalent and hydrogen bonds in the protein matrix, each having an associated electronic coupling factor.[1]

In comparison, inter-protein ET is less understood overall,[2–4] owing to the presence of the solvent and to the dynamic and transient nature of the protein–protein interaction and ET event. These features are averaged in space and time over protein ensembles in bulk measurements because of the intrinsic changes in relative position and mutual orientation between the redox protein partners. These experimental limitations prevent validating the diverse models of inter-protein ET that have been developed.[5] The current view is largely based on available co-crystal structures that show the bound mode and intimate (tunneling scale) contacts between the redox partners. These crystals are often obtained in conditions that favor binding and crystallization, like high molar ratio and ionic strength.[6] While these adjustments may be required to solve their atomic structure, they overlook the questions of whether that bound state represents the only possible ET-active configuration, and which are its associated dynamic processes. Other unanswered questions include: Can physiological ET between partners occur within the tunneling range at longer separations than required for binding? What is the energetic cost and kinetic delay of unbinding the active complex after ET?

Several laboratories have devised methods to accurately measure and model the charge transport properties of proteins (including not electroactive) in thick and monolayer films,[7,8] and as single entities.[9–12] Theoretical studies have shown the relevance of interfacial amino acids and bound water molecules in both the final protein–protein interaction orientation and interprotein ET coupling strength.[13,14] Experiments using solid-state molecular junctions of cytochrome c (Cc) proteins and self-assembled peptide monolayers mimicking the protein–protein interface confirmed that interfacial amino acids regulate the orientation and the energy barrier of interprotein ET.[15] Yet, compelling questions remain: Why non-redox proteins display high single-protein conductance?[9] What is the efficient mechanism that supports charge transport through tens of nanometers of protein layers in macroscopic experiments?[16–18] How can redox partners exchange current at long distances (>10 nm, rate $\beta \ll 5$ nm^{-1}) at the single protein level,[16,17] even in the absence of the metal cofactor?.[11]

The distance dependence of ET between the metal active site of a redox protein and an external probe has been studied using diverse approaches. They include cyclic voltammetry on metallic electrodes coated with self-assembled alkyl monolayers of controlled thickness,[19–21] and photoinduced ET with a ruthenium group that is chemically conjugated at specific protein residues.[22] However, these methods respectively measure ET through a non-aqueous medium and intra-protein ET, often constrained to tunnelable distances. Thus, although informative, they are not accurate models to study long-distance interprotein ET in aqueous physiological conditions. New insights have been obtained by wiring precisely oriented redox protein partners to the nanoscale electrodes of an electrochemical scanning tunneling microscope (EC-STM) via specific residues (cysteine) and measuring the current passage between them in aqueous solutions (**Figure 1a**; Figure S1bc, Supporting Information).[16–18,21] This setup differs from the biological scenario but gives unique control over the redox potential of the partners and their relative position and orientation at the single protein level and under adjustable quasi-physiological conditions.

Current-distance (I-z) recordings obtained in this way with electrochemical tunneling spectroscopy (ECTS) of Cc and its redox partner Cc_1 (the soluble fraction of cytochrome bc_1)

J. Samitier
Department of Electronics and Biomedical Engineering, Faculty of Physics
University of Barcelona (UB)
Barcelona 08028, Spain
C. Rovira, P. Gorostiza
Catalan Institution for Research and Advanced Studies (ICREA)
Barcelona 08010, Spain

provided experimental evidence of long-distance charge transport extending beyond 10 nm through the aqueous solution at pH = 6.6 (b ≈ 0.5 nm^{-1}).[16] Van der Waals interactions and electron tunneling cannot occur at these distances. I-z recordings depend on the electrochemical potential (gating)[16,23,24] and display maximum span around the partners' redox potentials. The long-distance currents are disrupted upon phosphorylation of a C*c* residue near the active site that is involved in biological regulation (Tyr48).[17] Both observations highlight the physiological relevance of the long-distance current observations. Molecular dynamics (MD) simulations in an explicit water model indicate that cations are depleted in the nanoscale gap between the partner proteins, thus preventing ionic charge screening and creating a local electric field in this region, described as Gouy-Chapman conduit (GCC).[16] These results can explain only in part the mechanism of long-distance charge transport through water. Although the establishment of a GCC follows classical electrostatics and agrees with basic physical chemistry notions, it does not suffice to explain long-distance currents. The major open question is the identity of the charge carriers being exchanged by the partners through this conduit and its associated electric field.

Hydrated electrons are exotic species in the biological context due to their short life and high energy.[25] Instead, candidate carriers must be stable in water, able to accept and donate electrons at moderate potentials, available in physiological media, and must be charged to drift in the GCC electric field. Here, we considered the involvement of protons and reactive oxygen species (ROS) in the charge exchange process between C*c* and Cc_1 and studied them with ECTS. We specifically tested whether I-z recordings are altered by the concentration of protons (pH), by changing their mass (using deuterons from heavy water, D_2O), and by the abundance of oxygen dissolved in the medium, which is the precursor of ROS.

We observe that the spatial span and electrochemical gating of long-distance currents are reduced at high pH. Currents are also less extended in D_2O and at low O_2 concentration. Based on the electrochemical processes that can be potentially mediated by ROS and protons in C*c* and Cc_1, we attribute these results to superoxide and to molecular hydrogen reactions assisted by proton-coupled electron transfer (PCET).

2. Results

We started by characterizing whether the ECTS current-distance relationship[24] between C*c* and Cc_1 depends on proton concentration. We used the cross complex between human C*c* (hC*c*) and the soluble domain of plant cytochrome c_1 (pCc_1), as previously described.[16,17] The experiments were conducted in 50 mM phosphate buffer within the pH range 6.6–8.0, which provides a 25-fold change in the proton concentration without introducing changes in the proteins' conformation and heme axial coordination.[26,27]

As depicted in Figure 1a, C*c* and Cc_1 were selectively immobilized on the probe and sample electrodes of the ECSTM, respectively. I-z recordings were obtained by placing the probe electrode on top of the sample at a fixed current set point (0.4 nA at constant bias of 200 mV), disconnecting the EC-STM feedback loop, and measuring the current decay at the probe while the piezoelectric scanner holding the probe was retracted at constant speed (12 nm·s^{-1}). The feedback loop was restored after each measurement, and the probe reapproached, allowing subsequent recordings at different sample locations. Faradaic leakage current was maintained below a few pA through probe insulation with apiezon wax.[28]

I-z plots were recorded at different probe (U_P) and sample (U_S) potentials versus a silver–silver chloride electrode (SSC), maintaining a constant bias of 200 mV. Distance decay rates (β, nm^{-1}) were quantified from the exponential region by fitting individual semilogarithmic I-z curves. For C*c*-Cc_1 in 50 mM phosphate buffer at pH = 6.5, we have reported that β values depend on the potential applied to the proteins (electrochemical gating), showing a minimum of $\beta = 0.6 \pm 0.3$ nm^{-1} at $U_S = 0.25$ V versus SCC (corresponding to a local work function F < 50 meV, in contrast to $\beta \approx 10$ nm^{-1}, F ≈ 0.8 eV between Au sample and Au probe in the same solution).[16,29,30] The minimum of β lies between the midpoint redox potentials of Cc_1 (0.28 V vs SSC) and C*c* (0.35 V vs SSC), thereby indicating 1) that the metal centers participate in the electron transport process when the Fermi energy of the electrodes is aligned with them, and 2) that this electrochemical gating[21] effect is relevant for the biological function of the proteins.[16,17]

Similar experiments at pH between 6.6 and 8.0 showed that the electrochemical potential gating of β is weaker upon increasing pH (lower proton concentration), leveling off progressively at 1–2 nm^{-1} (Figures S2–S5, Supporting Information). The β distributions at different potentials are multimodal at pH = 7.4, whereas they are single modal and do not depend on the applied potential at pH = 8.0. Although long-distance currents are observed at $U_S = 0.25$ V versus SCC in all conditions, β is significantly higher at higher pH values, thus implying less efficient electron transport (Figure 1b,c).[31] The β at pH = 6.6 is 2.5 times smaller than at higher pH, while no significant differences are observed between β at pH = 7.4 and pH = 8.0. These results cannot be explained by a direct electron tunneling process and suggest that protons participate in the transport between Cc_1 and C*c*.

To further investigate this dependence, we studied the role of the proton mass in ECTS I-z measurements by using deuterated water (deuterons) at similar pH and pD values, set with dehydrated phosphate buffer salts. A correction of +0.41 was applied to the pH of buffer solutions in heavy water measured with conventional glass electrode, to convert them into pD values.[32,33] We recorded I-z curves at different probe and sample potentials in D_2O at pD = 6.9 (Figure S6, Supporting Information). At $U_S = 0.25$ V versus SSC, $U_P = 0.45$ V versus SSC (bias 200 mV, 0.4 nA initial setpoint), the current is reduced more steeply with the distance in D_2O than in H_2O, and the distribution of β values is significantly broader (**Figure 2a**) showing a main peak at 0.9 ± 0.3 nm^{-1} and two new components at 2.4 ± 0.4 nm^{-1} and at 6 ± 2 nm^{-1} (Figure 2b). The shift of the main peak to higher values of β indicates that D_2O increases the energy toll of the C*c*-Cc_1 interaction and hence the probability of alternative electron transport pathways (e.g., through the protein and through the solution), which would account for the appearance of the new high-β components. Similar results have been obtained with another redox protein in D_2O using bulk measurements.[21] The different β values obtained in H_2O and D_2O cannot be explained by a tunneling mechanism and confirm the role of protons in the process.

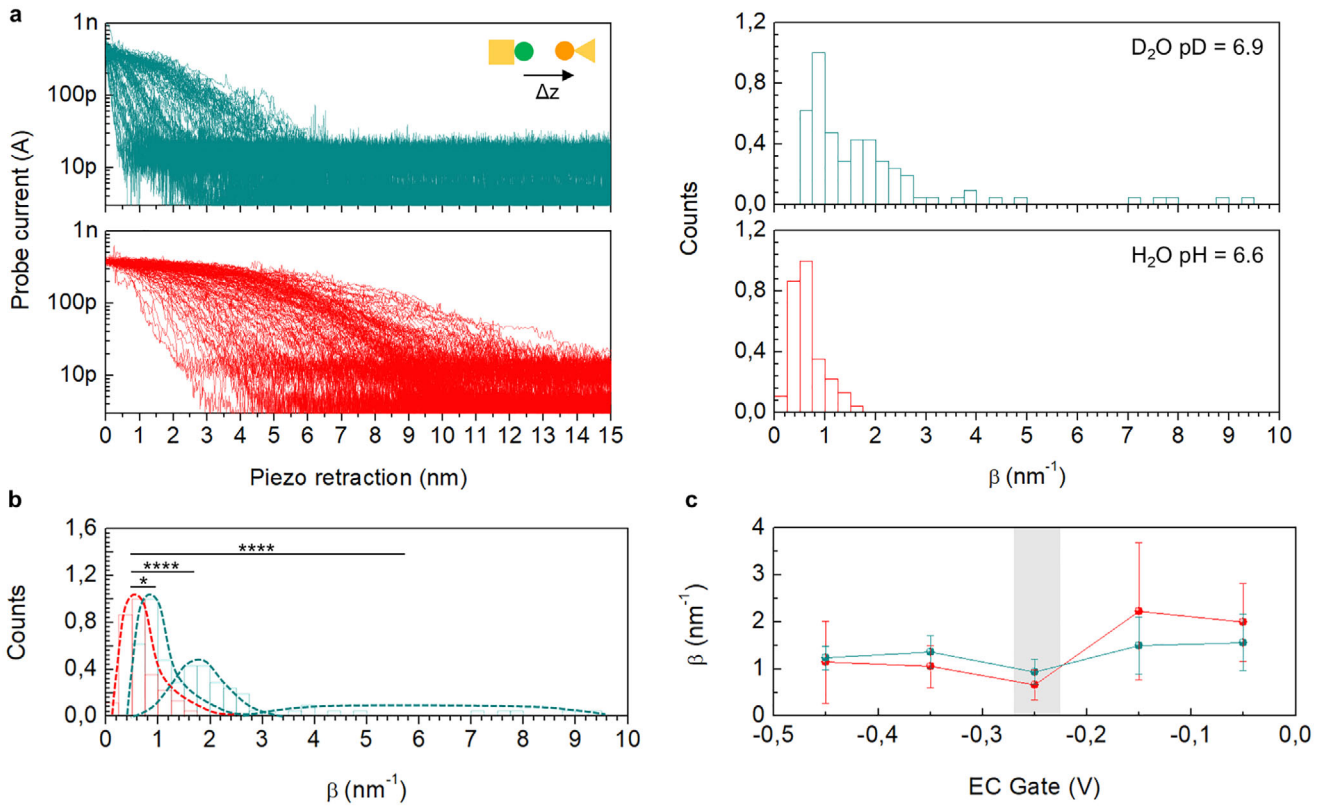

Figure 2. Current-distance electrochemical tunneling spectroscopy of C*c*-C*c*$_1$ in deuterated water (D_2O). a) (Left) Ensemble of semi-logarithmic I-z curves obtained for C*c*-C*c*$_1$ in 50 mM phosphate D_2O buffer solution of pD = 6.9 (green), and in 50 mM phosphate buffer aqueous solution pH 6.6 (red). Sample and probe electrodes are represented by a square and a triangle with bound C*c*$_1$ and C*c*, respectively. (Right) The corresponding β histograms quantified from individual I-z curves. b) Comparison of β distributions (one-way ANOVA with Tukey's multiple comparisons post hoc test, $\alpha = 0.05$, *$p < 0.05$; ****$p < 0.0001$). c) Averaged β values (mean ± s.d. of n_{H2O} at least 57, n_{D2O} at least 61, $N = 2$) versus the electrochemical gate potential.[34] The gray area corresponds to the region comprised between the midpoint redox potentials of C*c*$_1$ at the sample (0.28 V vs SSC) and of C*c* at the probe (0.35 V vs SSC), respectively.

The potential dependence (gating) is also reduced in D_2O (Figure 2c; Figure S6, Supporting Information). Since the EC-STM probe is grounded in our EC-STM configuration, the potential of the reference electrode is adjusted to modulate the sample potential (U_S), in an analogous way to the gate electrode in a field effect transistor. Therefore, here -U_S can be taken as the gate voltage at any given bias.[34]

The results of Figure 2 allow calculating the kinetic isotope effect (KIE, i.e., the ratio of reaction rates in the lighter over the heavier solvent)[19,20,35–37] using the electron rates given by the EC-STM current,[24] which are proportional to $e^{-\beta \cdot z}$. Taking the β peak values at pH = 6.6 and pD = 6.9 (Figures 1 and 2) and considering $I_{H2O} / I_{D2O} = e^{(\beta(D2O) - \beta(H2O)) \cdot z}$, the kinetic isotope effect yields 1.3, 4.5, and 20 at arbitrary distances 1, 5, and 10 nm, respectively, in agreement with previous reports using other methods.[34–37]

We also conducted current-time (I-t) "blinking" measurements to account for the spontaneous interaction between C*c*$_1$-C*c* (**Figure 3**). In I-t recordings, the probe of the ECSTM is positioned above the sample at the current set point (0.3 nA), the feedback loop is transiently disconnected, and the probe current is recorded versus time at a constant bias (U_{bias} = 800 mV, U_S = −0.2 V vs SCC, U_p = 0.6 V vs SSC, Figure 3a).[17,34,38,39] Spontaneous interaction between the probe-C*c* and the sample-C*c*$_1$ resulted in transient current jumps (blinks), which can be attributed to the net conductance established during the protein partners' interaction (Figure 3b). The collected blink currents (current at each blinking event) were set to a common time origin (initial blinking time = 0), and after subtracting the baseline current, they were plotted in 2D-histograms with the blinking lifetimes (time duration of the blinks). 2D-blinking maps show the most probable conductance ($G = I_{blink} / U_{bias}$) and lifetime values for C*c*$_1$-C*c* in H_2O and D_2O (Figure 3c). The C*c*-C*c*$_1$ conductance distribution measured in D_2O shows two equiprobable populations peaking at $2.4 \cdot 10^{-6}$ G_0 and $8.9 \cdot 10^{-6}$ G_0, in contrast to the most probable conductance at $4.3 \cdot 10^{-6}$ G_0 obtained in H_2O. D_2O also displayed longer lifetime values, indicating the formation of more stable junctions (40 ms vs 30 ms in D_2O and H_2O, respectively). These results may be related to the fact that replacing H_2O by D_2O reduces the protein backbone flexibility,[10] and increases the propensity to form hydrogen bonds between residues instead of between water and the protein.[40–42] This could allow protein partners to get closer and charge transport to occur mainly through protein backbones leading to a higher conductance interaction, as previously observed for the phosphomimetic Cc.[17]

To get further insights into the role of protons in the electron transport between C*c* and C*c*$_1$, we examined the pK_a of their

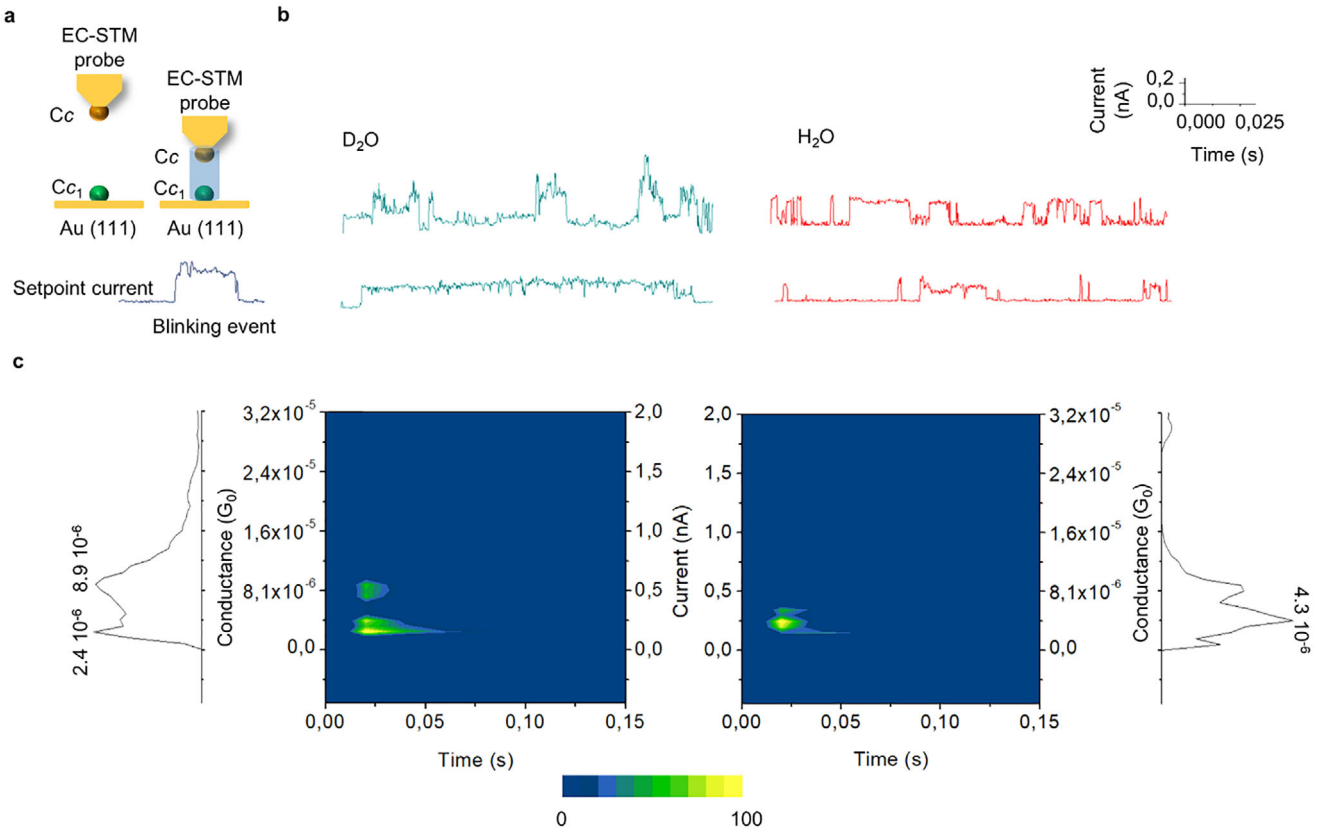

Figure 3. Current-time measurements in water and deuterated water. a) Scheme of the current-time (I-t) measurement between C*c* and Cc_1 in the EC-STM showing C*c* (orange) bound to the EC-STM probe and Cc_1 (green) bound to the Au(111) electrode surface. b) Representative I-t recording for C*c*-Cc_1 in 50 mM phosphate D_2O buffer solution of pD 6.9 (green), and in 50 mM phosphate buffer aqueous solution pH 6.6 (red). c) 2D histograms of blink current and blink lifetime (n_{D2O} = 166 095 and n_{H2O} = 100 980 conductance values included). Counts are normalized and represented on a color scale. $G_0 = 2e^2/h = 77.5$ µS, with *h* the Planck constant and *e* the electron charge.

amino acid side chains, i.e., their ability to undergo proton exchange reactions with the solution. Calculating the pK_a of protein residues is a necessary step to assign charges and prepare proteins for molecular dynamics studies.[43–45] We used H^{++}[46] and PropKa3.5[47] to predict the pK_a values of the reduced and oxidized C*c*[48] (Protein Data Bank accession numbers 2N9I and 2N9J, respectively; pH = 6.8). Several residues display differences with respect to the protein redox state that are larger than one pH unit, which is generally regarded to be significant in these calculations.[47] These results are shown in **Figure 4**a,b for H^{++}. Although the agreement between H^{++} and PropKa3.5 predictions is only partial (see Spreadsheet S1, Supporting Information), they reach a consensus set of four residues, which are labeled in green in the oxidized structure of Figure 4c (Lys13, Tyr46, Lys79, Asp93; see also Tables S1 and S2, Supporting Information). Thus, we identify a network of ionizable sites whose protonation state is linked to the protein redox state, which means that they can switch their availability to form hydrogen bonds with water and/or to mediate proton-coupled electron transfer (PCET) reactions.[37,49–52] Coupling of the C*c* redox reaction with proton-transfer steps has been observed by surface-enhanced Raman spectroscopy and attributed to the rearrangement of the hydrogen-bonding network of the protein.[20] The residues of Figure 4c are located around or near the solvent-exposed heme active site and all residues in C*c* are located at <2 nm (i.e., tunneling distance) from the iron ion in the heme group (Spreadsheet S1, Supporting Information). The amino acids of Figure 4 are partially conserved across prokaryotic and eukaryotic organisms, which indicates the importance of their function (Figure S7, Supporting Information). These simple calculations based on high-resolution experimental structures suggest that the redox and protonation states of C*c* are coupled, i.e., that electron exchange facilitates hydrogen bonding and/or proton exchange with water, and vice versa. Near the extended electric field of the GCC, these processes might lead to long-distance charge transport between the redox partners through the aqueous solution.

Next, we examined the effect of oxygen (O_2) dissolved in the aqueous solution, which can participate in redox reactions and give rise to ROS.[53] ECTS experiments do not allow simultaneous degassing of the solution by argon bubbling due to the generation of mechanical vibrations. They also require an antivibration system that is complex to combine with a glove box for continuous operation at low O_2 concentration. As an alternative, we filled the microscope chamber with a previously degassed solution and used solution conductance measurements to determine that atmospheric dissolved O_2 levels are restored in ≈20 min in the closed, non-hermetic, argon-filled EC-STM chamber (see Experimental Section). Thus, we performed I-z recordings as a function

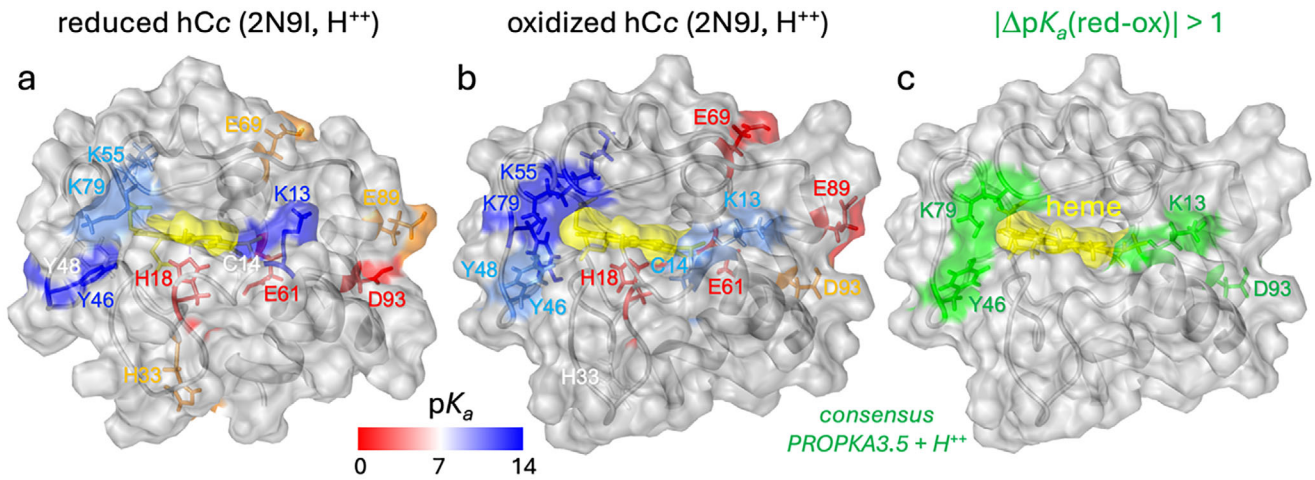

Figure 4. Residues displaying redox-dependent pK_a in C*c*. Front view of the C*c* active site displaying the heme group in yellow. The pK_a values of each residue were calculated using H^{++} in reduced (a) and oxidized (b) C*c* structures[48] and represented using a color code (see Spreadsheet S1, Supporting Information). Twelve residues out of 103 display a difference in pK_a higher than one pH unit between the reduced and oxidized forms (see Spreadsheet S1, Supporting Information). Four of them agree with the predictions of PropKa3.5 (green in panel c). Since all C*c* residues are at tunneling distance from the heme site, this network of redox-dependent (de)protonating sites can switch its availability to form hydrogen bonds with water and/or to mediate PCET reactions, leading to long-distance charge transport between the redox partners along the extended electric field of the GCC.

of time and compared those obtained in the first and in the last 10 min as corresponding to low and high O_2 concentration, respectively. They are plotted in grey and black, respectively, in **Figure 5** and show that the spatial span of I-z plots is lower at low O_2 conditions (initial setpoint 0.4 nA, constant bias 200 mV, U_S = 0.25 V vs SSC, U_P = 0.45 V vs SSC). We observe that β values significantly increase in the degassed solution ($\beta = 1.9 \pm 0.8$ nm^{-1}; n = 119 for <10 min, and n = 130 for >10 min, N = 2, Mann Whitney test, U = 5400, two-tailed, ****$p < 0.0001$) and are progressively reduced after 10 min of recording. Thus, O_2 or its ROS byproducts are also involved in long-distance charge transport between C*c* and Cc_1.

3. Discussion

Using ECTS at different pH values, in D_2O, and in ambient and deoxygenated conditions, we identify protons and oxygen species as carriers and/or mediators of interprotein long distance charge transport between C*c* and Cc_1 through the aqueous solution.

C*c* is known to display oxygen-dependent redox activity,[53,54] and it has been used as an electrochemical ROS sensor, most notably of superoxide anions ($O_2^{-}\cdot$).[54] Superoxide is formed by direct reduction of oxygen at moderate redox potentials ($O_2 + e^- \rightarrow O_2^{-}\cdot$, −0.54 V vs SSC).[55] Oxygen can also yield H_2O_2 and HO_2^- (notably by C*c* at pH < 4 and in the presence of

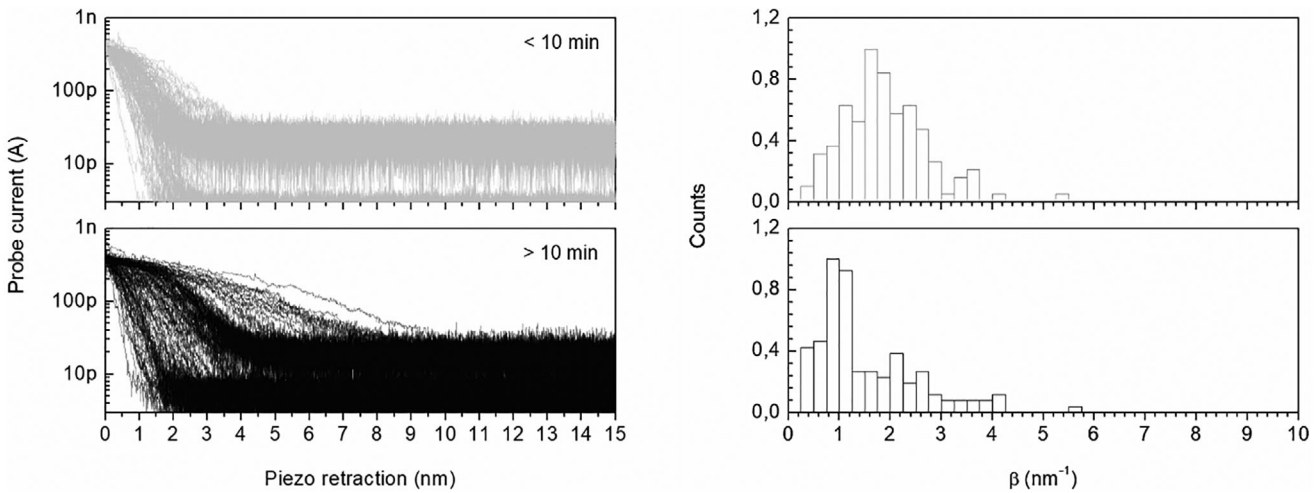

Figure 5. Effect of O_2 concentration in the current-distance decay between Cc_1-C*c*. Ensemble of semi-logarithmic I-z curves (left), and the corresponding β histograms (right) of C*c*-Cc_1 in 50 mM phosphate buffer at pH 6.6, obtained during the first 10 min of recording (grey, n = 119, N = 2) and after 10 min (black, n = 130, N = 2). The buffer was degassed with nitrogen for >1 h before the measurements, and the experiment was conducted under argon atmosphere in the closed EC-STM chamber (non-hermetic). Comparison of the β distributions leads to statistically significant differences (Mann–Whitney test, U = 5400, two-tailed, ****$p < 0.0001$).

cardiolipin), but these reactions involve two electrons, and the charged product is not stable at neutral and acidic pH.[56] Since superoxide is stable in neutral and acidic water, charged, and can exchange electrons with C*c*[55] and Cc_1,[57] it could drift along the interprotein GCC electric field[16] toward C*c* and mediate electron transport between the partners, giving rise to the results observed in Figure 5. Superoxide anion is a common byproduct in complex I and complex III. In particular, superoxide produced at the ubiquinol oxidation center (center P, Qo site) of complex III has additional physiological functions as signaling molecule.[58] Superoxide in complex III can be released either to the mitochondrial matrix and intermembrane space, where it could aid ET between Cc_1 and C*c* in physiological conditions, thus acting as a "silent mediator" by means of a futile redox cycle[59] (being oxidized at C*c* and reduced at Cc_1).

However, protons do not participate in superoxide formation and cannot account for the observed pH dependence. The presence of protons favors the span and redox selectivity of long-distance charge transport (Figures 1–3; Figures S2–S5, Supporting Information). Although cyclic voltammetry of electrode-bound C*c* displays weak pH dependence[60] that does not reveal a primary role of protons in ET,[61,62] local pH has not been studied in nanoscale environments in this system and could have gone unnoticed. Protons are charged and can either drift along the GCC electric field away from C*c* or be effectively transported by a classical Grotthuss mechanism of proton hopping conduction,[63–66] accounting for the results of Figures 1–3.

However, the redox reactions of direct proton reduction and hydrogen oxidation at neutral pH (−0.63 V vs SSC) involve two electrons and are difficult to attain under physiological conditions. They might occur indirectly if protonation of a pair of residues (e.g., near the Fe site) can lower the energy barrier enough for the reduction reaction to occur, but the reported facilitation of hydrogen evolution in electrodes modified with protonating amino acids is limited, at least in the absence of the heme.[67] In either case, the hydrogen reactions would involve coupling between the redox and protonation states of the proteins (PCET), by means of the ionizable residues discussed in Figure 4. Thus, protons could act as another silent mediator of electron transport between C*c* and Cc_1. Note that, lacking charge, molecular hydrogen potentially produced at Cc_1 should rely on diffusion to reach C*c* and to close the reaction cycle. Thus, it could also leak away from the partners and out of mitochondria, partially accounting for the intriguing hydrogenase activity that is currently being investigated.[68]

The effect of pH (Figures 1–3) can also be caused by the residues identified in Figure 4 switching their availability to form hydrogen bonds with water as a function of the protein redox state, thus initiating Grotthuss proton transport.[51,63] This mechanism is favored at slightly acidic to neutral pH, where H^+ mobility increases due to the combination of proton availability and stability of hydrogen-bond networks for H^+ hopping.[63] However, the large KIE values obtained suggest a strong coupling between proton and electron reactions and cannot be attributed to classical proton transfer. They can be indicative of hydrogen atom transfer and proton tunneling (much more sensitive to mass),[69] which are generally associated to short-distance mechanisms in membrane transporter proteins.[69–73] In our case, they could support ET through the solvent at long distances using structured water confined between Cc_1-C*c*, which facilitates Grotthuss proton hopping while still providing a polarizable medium for ET.[51] The presence of water near redox cofactors has been reported to accelerate ET kinetics through the formation of strongly coupled, constructively interfering ET pathways, influencing electrostatic environments, and dynamically modulating the ET efficiency.[13,14,16,74,75]

Potential candidates to act as PCET sites are Cys14 (binding to the heme prosthetic group), His18, and Tyr67 (coordinating the iron ion as axial ligands), which are predicted by either H^{++} or PropKa3.5, but not both, and thus are not labeled green in Figure 4c. Consensus Lys79 is known to replace the axial heme ligand Met80 above the alkaline transition at pH = 9.5. Due to the nanometric size of C*c*, all its residues are located at tunneling distances from the heme and could in principle engage in PCET reactions if they can exchange protons. Indeed, the concept of PCET via hydrogen-bonding networks is well established.[20,76–78]

In particular, histidine bears an imidazole group whose deprotonated form has two tautomers and plays important roles as catalytic site and proton shuttle in enzymes.[79] The redox-dependent pK_a of Tyr46 may facilitate inter-protein charge transport[15] and PCET like other tyrosine residues undergoing oxidation/reduction reactions in photosystem II and ribonucleotide reductase.[80] Note that the nearby Tyr48 (identified by H^{++}) is involved in C*c* regulation by phosphorylation and is known to reduce the pK_a of Met80 from 9.5 to 7.8.[17,81] The consensus Lys13 is included in the lysine ring that interacts with complex III and is important for fast ET.[82,83] In contrast, Asp93 is located farther from the heme and its function is currently unknown.

We noticed that this network of conserved residues displaying redox-dependent changes in pK_a (Figure 4; Figure S7, Supporting Information) form a streak that might be related to the entry and exit path of the C*c*-complex III interaction and/or to the alignment of multiple C*c* carriers, as proposed for this system[84,85] and for the interaction between cytochrome c_2 and its molecular partners.[86–88] The redox-dependent pK_a of the heme ligands may also cause the reported opening of the heme crevice in oxidized C*c*[89] that is observed in the structures of Figure 4.

Overall, we propose that the proton donor and acceptor sites are the ionizable amino acids of C*c* and Cc_1 respectively, whose pK_a depends on the redox state (Figure 4). All of them are located over the protein surface at tunneling distances (< 2 nm) from the metal centers (Figure 4) such that changes in the protein redox state can be coupled to the exchange of protons with the solution. The released proton can drift along the electric field of the GCC between C*c* and Cc_1[16] and/or be transported by a Grotthuss hopping mechanism. In either case, it gives rise to a measurable current between the probe and sample electrodes that decays over long distances (low β decay rate).

These interpretations of the experimental results should be taken with caution. First, the identity of the ionizable residues of Figure 4 could be verified by constant pH molecular dynamics or free energy perturbation calculations in explicit water solvent (possibly including water dissociation), with the heme, and ideally using mutations that do not compromise protein stability and yield simple phenotypes. Some redox-dependent changes in pK_a correspond to relatively acidic and basic pH values

(Table S1, Supporting Information), which question their relevance under physiological conditions at neutral pH. However, the ability of these residues to exchange protons may intrinsically alter the local pH around them.[90] The moderate potential that is locally applied in ECTS experiments could favor proton exchange and/or ROS reactions with the proteins.

And last, the effects of D_2O might be partially due to the lower hydrogen bonding between these solvent molecules and C*c* side chains (e.g., lysines), which can increase the availability of these residues to interact with Cc_1, leading to more stable protein–protein complexes and longer blink events than in H_2O (Figure 3).[42]

Nevertheless, our observations unveil the intrinsic ability of C*c* and Cc_1 to carry pH- and oxygen-dependent long-distance currents through the aqueous solution in the reported experimental conditions. The interpretations of these single molecule experiments could be tested with specially designed bulk measurements.

Transporting charge between protein partners at a distance through the solution can not only reduce the force and duration of the interaction,[17] but also expose it to the local environment and render it susceptible to biological regulation by a convenient diversity of ways. Protons and superoxide anions are important reactants and byproducts of respiratory chain enzymes. Coupling their local concentrations to the rate of electron transport between respiratory complexes offers direct mechanisms of "electrochemical feedback" for homeostatic regulation under relevant environmental situations in the cell. Interaction with quinones, flavins, and nicotinamide adenine dinucleotide may also be relevant in vivo. Understanding the detailed mechanisms of proton exchange and charge transport dynamics in proteins and materials is fundamental for biochemistry and to develop advanced protonic devices.[91–95]

4. Conclusion

To identify the charge carriers involved in long distance charge transport between C*c* and Cc_1, we have performed ECTS (I-z and I-t) recordings as a function of pH, in the presence of D_2O, and at reduced O_2 concentration in the aqueous solution. We have observed currents between C*c*- and Cc_1-functionalized electrodes spanning over very long (>10 nm) distances that depend on the proton and oxygen concentrations and that are not compatible with direct electron tunneling mechanisms. Using experimental structures of oxidized and reduced C*c* and pK_a calculations, we have also identified residues that can switch their availability to form hydrogen bonds with water and/or engage in PCET reactions. Our results indicate that long distance currents between C*c* and Cc_1 through the aqueous solution are assisted by protons and superoxide anions in the evaluated experimental conditions. We propose possible molecular mechanisms for these reactions and discuss their feasibility and biochemical relevance for ET in respiratory complexes.

5. Experimental Section

Protein Preparation: *Escherichia coli* BL21 (DE3) cells were transformed with pBTR1-E104C plasmid to express *Homo sapiens* E104C C*c* in a recombinant way and it was purified as previously described.[96] The soluble domain of *Arabidopsis thaliana* Cc_1 was expressed and purified as described,[83] with minor modifications. *E. coli* BL21 (DE3) cells co-transformed with the plasmids pET_pCc_1 and pEC86 were used to produce the soluble form of Cc_1. E104C C*c* and Cc_1 samples were dialyzed against 10 mM sodium phosphate, pH between 6.5 and 7.0.

Sample Preparation: Atomically flat Au(111) single-crystal disks of 9 mm diameter and 1 mm thickness (MaTecK) were flame annealed and electrochemically polished prior to use.[34] They were incubated with Cc_1 in sodium phosphate buffer 10 mM, pH = 6.5 at a 56 µM concentration. ECSTM probes were mechanically cut from a gold wire of 0.25 mm in diameter (GoodFellow) and were insulated with Apiezon wax.[24] The probes were incubated with a 12.5 µM solution of C*c*, in sodium phosphate buffer 10 mM, pH = 6.5. All incubations were conducted overnight and at 4 °C. Working solutions were phosphate-buffered. They were prepared from 0.2 M solutions of sodium phosphate monobasic ($H_2NaO_4P.H_2O$, Merck) and sodium phosphate dibasic ($HNa_2O_4P{\cdot}2H_2O$, Merck). The pH and pD values of buffer solutions were verified on a pH-Meter BASIC 20+ pH meter (Crison) calibrated with two standard buffer solutions. pH readings were converted to pD by adding 0.4 units.[32,33] All solutions were filtered through 0.02 µm diameter sterile membrane (Whatman Anotop syringe filters, Merck). To study the effect of dissolved O_2, solutions were degassed by bubbling 99.99% N_2 and kept in an argon atmosphere without constant flow, to avoid mechanical vibrations that affect ECSTM performance. The concentration of O_2 was measured with a conductance meter (Crison EC-Meter Basic 30+) using tabulated values,[97,98] which yield 8 mg L^{-1} under ambient conditions and <1 mg L^{-1} after degassing with 99.99% N_2 for 1 h.[99,100]

ECSTM Measurements: All experiments were performed with a Molecular Imaging PicoSPM microscope head and a PicoStat bipotentiostat (Agilent) controlled by Dulcinea electronics (Nanotec Electronica), and data were acquired using WSxM 4.0 software. A homemade electrochemical liquid cell with a standard sample plate was used in four-electrode configuration, using a 55 mm length, 0.25 mm diameter $Pt_{80}Ir_{20}$ wire as a counter electrode and a miniaturized ultralow leakage membrane Ag/AgCl (SSC) reference electrode filled with 3 M KCl (WPI, reference DRIREF-2SH). The potentials of the Au(111) electrode sample (U_S) and EC-STM probe (U_P) are expressed against this reference. Prior to measurements, the electrochemical cell and the counter electrode were cleaned with piranha solution (3:1 v/v solution of H_2SO_4 and H_2O_2). *Caution: piranha solution is a strong oxidizer and a strong acid. It should be handled with extreme care, as it reacts violently with most organic materials*. I-z curves were acquired by setting an initial current set point of 0.4 nA, turning the feedback loop off, and recording the probe current at 12 nm·s^{-1} during probe retraction along 15 nm (20 samples per point, 1024 points) at a constant bias ($U_{bias} = U_P - U_S$) of 200 mV (U_S = 0.25 V, U_P = 0.45 V vs SSC). Data were treated with the custom-generated MATLAB code (The Mathworks, Inc.) previously reported.[16]

For static blinking experiments, a NI-DAQmx and BNC-2110 LabVIEW setup was used for data acquisition. The STM probe was set at a 0.3 nA current set point, and at a constant bias of 800 mV ($U_S = -0.2$ V, $U_P = 0.6$ V vs SSC), and the feedback was turned off after a period of mechanical stabilization. Current versus time traces were then recorded in captures of few seconds during several hours. The current was transformed to conductance values using $G = I_{blink}/U_{bias}$. The data was treated with LabVIEW software.

Statistical Analysis: Data were analyzed with OriginPro 8.5.0 SR1 (OriginLab Corp.). Statistics were performed using Graphpad Prism v.8. Samples were subjected to a normality test and significant differences were judged using the corresponding parametric or nonparametric tests. An α of <0.05 was considered statistically significant. At least 2 independent experiments were conducted in each case, where "n" indicates the sample size. Errors are displayed as standard deviation of the mean.

Computational pK_a Calculations: The protonation states of Cc residues in its oxidized and reduced form were predicted using two different approaches (see the results in Figure 4 and Supplementary Table online). First, the H^{++} server (version 4.0)[46,101] was used with the following parameters: internal and external dielectric constants were set to 10 and 80, respectively, and the ionic strength was set to 0.05 M. The calculations

were performed at pH 6.8, consistent with the NMR experimental conditions. The input structures (PDB ID: 2N9I and 2N9J)[48] were preprocessed by mutating Glu104 to Cys to match the experimental system, and all hydrogen atoms were removed to allow full protonation state prediction. Model 1 from each NMR ensemble was selected for the calculations. As a complementary approach, PropKa 3.5[47] was employed using the same structures and conditions (pH 6.8, ionic strength 0.05 M). PropKa estimates the pK_a values of ionizable groups using empirical rules that consider desolvation effects and intramolecular interactions. Residues displaying a predicted change in the absolute value of pK_a above one unit by both H^{++} and PropKa 3.5 ("consensus") are shown in green in Figure 4, Figure S7 (Supporting Information), online Supplementary Table, and discussed in the text.

Sequence Alignments and Residues Conservation: The protein sequence from human C*c* (PDB: 2N9I) was used as a reference structure to identify C*c* proteins across multiple model organisms by running BLASTP on the non-redundant protein sequences database.[102] From over one hundred returned sequences (with >90 % sequence similarity), eleven C*c* sequences representing different species were selected. The alignment analysis was performed using Clustal Omega[103] and was subsequently plotted and refined with JalView.[104,105]

Supporting Information

Supporting Information is available from the Wiley Online Library or from the author.

Acknowledgements

The authors are grateful to Julea N. Butt, Marilyn Gunner, David Waldeck, Leif Hammarström, Alonso Gamero-Quijano, Jens Ulstrup, Ana Moore, Thomas Moore, Brian M. Hoffman, Nongjian Tao, Szilveszter Gaspar, Fred Lisdat, Antoni Llobet, Sharon Hammes-Schiffer, Philippe Allongue, Marcel Rost, Gunther Wittstock, David Cahen, Sung Sakong, Ulrich Stimming, Ángel Cuesta, Ulrike Diebold, Fouad Maroun, Miguel Machuqueiro, Inês Pires, Kristina Tschulik, Christian Durante, and Peng Chen for helpful discussions. The authors thank Albert Cortijos, Isabel Oliveira, and David Izquierdo for technical support. This research was supported by the Government of Catalonia (CERCA Program; AGAUR 2021-SGR-01410, 2021-SGR-01545, and 2021-SGR-00680); by the Spanish Ministry of Science and Innovation (grants AEI / 10.13039 / 501100011033; PID2021-126663NB-I00 and PID2024-157414NB-I00; Research Network in Biomedicine eBrains-Spain, RED2022-134823-E; PID2020-118893GB-100, CEX2021-001202-M, a postdoctoral fellowship Margarita Salas to A.N.-H., a postdoctoral fellowship POSTD.O.C_21_00395, financed by the Junta de Andalucía /CUII and by the ESF+′ to A.G.-C., and the Complementary Plan of Biotechnology applied to Health coordinated by IBEC within the framework of Recovery, Transformation, and Resiliency Plan (C17.I1) funded by the European Commission NextGenerationEU); by the EU Horizon 2020 Framework Programme for Research and Innovation (including the European Innovation Council Pathfinder (Phototheraport, 101130883), and Information and Communication Technologies (Deeper, ICT-36-2020-101016787)); and by the Networking Biomedical Research Center (CIBER is an initiative funded by the VI National R&D&i Plan 2008-2011, Iniciativa Ingenio 2010, Consolider Program, CIBER Actions and the Instituto de Salud Carlos III, with the support of the European Regional Development Fund ERDF); and by Ramón Areces Foundation (LEUCYTO-FRA2025-MAR).

Conflict of Interest

The authors declare no conflict of interest.

Data Availability Statement

The data that support the findings of this study are available from the corresponding author upon reasonable request.

Keywords

electrochemical STM, Gouy-Chapman conduit, Grotthuss (Grothuss) proton hopping conduction, kinetic isotope effect KIE, mitochondria, proton coupled electron transfer PCET, reactive oxygen species ROS, superoxide radical anion SOX

Received: January 31, 2025
Revised: August 14, 2025
Published online: September 12, 2025

[1] W. B. Curry, M. D. Grabe, I. V. Kurnikov, S. S. Skourtis, D. N. Beratan, J. J. Regan, A. J. A. Aquino, P. Beroza, J. N. Onuchic, *J. Bioenerg. Biomembr.* **1995**, *27*, 285.
[2] G. McLendon, R. Hake, *Chem. Rev.* **1992**, *92*, 481.
[3] C. C. Moser, C. C. Page, R. Farid, P. L. Dutton, *J. Bioenergetics Biomembr.* **1995**, *27*, 263.
[4] D. S. Bendall, in *Protein Electron Transfer*, Taylor and Francis Group, Oxfordshire, UK **2020**.
[5] C. Page, *Curr. Opin. Chem. Biol.* **2003**, *7*, 551.
[6] T. Kawakami, L.-J. Yu, T. Liang, K. Okazaki, M. T. Madigan, Y. Kimura, Z.-Y. Wang-Otomo, *Nat. Commun.* **2021**, *12*, 1104.
[7] S. Bera, J. A. Fereiro, S. K. Saxena, D. Chryssikos, K. Majhi, T. Bendikov, L. Sepunaru, D. Ehre, M. Tornow, I. Pecht, A. Vilan, M. Sheves, D. Cahen, *J. Am. Chem. Soc.* **2023**, *145*, 24820.
[8] D. Cahen, I. Pecht, M. Sheves, *J. Phys. Chem. Lett.* **2021**, *12*, 11598.
[9] B. Zhang, E. Ryan, X. Wang, S. Lindsay, *J. Am. Chem. Soc.* **2021**, *143*, 15139.
[10] S. Afsari, S. Mukherjee, N. Halloran, G. Ghirlanda, E. Ryan, X. Wang, S. Lindsay, *Nano Lett.* **2023**, *23*, 8907.
[11] M. López-Ortiz, R. A. Zamora, M. I. Giannotti, P. Gorostiza, *ACS Nano* **2023**, *17*, 20334.
[12] Z. Zhao, N. Kostopoulos, S. Ganguli, P. Bergstrom, A. Sekretareva, *ChemRxiv* **2024**, https://doi.org/10.26434/chemrxiv-2024-q12fw-v3.
[13] J. Lin, I. A. Balabin, D. N. Beratan, *Science* **2005**, *310*, 1311.
[14] A. de la Lande, N. S. Babcock, J. Řezáč, B. C. Sanders, D. R. Salahub, *Proc. Natl. Acad. Sci. USA* **2010**, *107*, 11799.
[15] Y. Zhang, H. Liang, P. Qi, Z. Xu, H. Fei, C. Guo, *Nano Lett.* **2024**, *24*, 4178.
[16] A. Lagunas, A. Guerra-Castellano, A. Nin-Hill, I. Díaz-Moreno, M. A. De la Rosa, J. Samitier, C. Rovira, P. Gorostiza, *Nat. Commun.* **2018**, *9*, 5157.
[17] A. M. J. Gomila, G. Pérez-Mejías, A. Nin-Hill, A. Guerra-Castellano, L. Casas-Ferrer, S. Ortiz-Tescari, A. Díaz-Quintana, J. Samitier, C. Rovira, M. A. De la Rosa, I. Díaz-Moreno, P. Gorostiza, M. I. Giannotti, A. Lagunas, *Nat. Commun.* **2022**, *13*, 7100.
[18] M. López-Ortiz, R. A. Zamora, M. I. Giannotti, C. Hu, R. Croce, P. Gorostiza, *Small* **2022**, *18*, 2104366.
[19] D. E. Khoshtariya, J. Wei, H. Liu, H. Yue, D. H. Waldeck, *J. Am. Chem. Soc.* **2003**, *125*, 7704.
[20] D. H. Murgida, P. Hildebrandt, *J. Am. Chem. Soc.* **2001**, *123*, 4062.
[21] Q. Chi, O. Farver, J. Ulstrup, *Proc. Natl. Acad. Sci. USA* **2005**, *102*, 16203.
[22] H. B. Gray, J. R. Winkler, *Proc. Natl. Acad. Sci. USA* **2005**, *102*, 3534.
[23] D. Vanmaekelbergh, A. J. Houtepen, J. J. Kelly, *Electrochim. Acta* **2007**, *53*, 1140.
[24] J. M. Artés, I. Díez-Pérez, F. Sanz, P. Gorostiza, *ACS Nano* **2011**, *5*, 2060.
[25] J. L. Dye, *Science* **2003**, *301*, 607.
[26] T. Ying, F. Zhong, J. Xie, Y. Feng, Z.-H. Wang, Z.-X. Huang, X. Tan, *J. Bioenerg. Biomembr.* **2009**, *41*, 251.

[27] J. J. Osterhout, K. Muthukrishnan, B. T. Nall, *Biochemistry* **1985**, *24*, 6680.
[28] A. G. Güell, I. Díez-Pérez, P. Gorostiza, F. Sanz, *Anal. Chem.* **2004**, *76*, 5218.
[29] M. J. Rost, in *Encyclopedia of Interfacial Chemistry*, Elsevier, Amsterdam, The Netherlands **2018**, pp. 180.
[30] N. S. Wigginton, K. M. Rosso, A. G. Stack, M. F. Hochella, Jr., *J. Phys. Chem. C* **2009**, *113*, 2096.
[31] M. Hugelmann, W. Schindler, *Surf. Sci.* **2003**, *541*, L643.
[32] A. K. Covington, M. Paabo, R. Anthony Robinson, R. G. Bates, *Anal. Chem.* **1968**, *40*, 700.
[33] P. K. Glasoe, F. A. Long, *J. Phys. Chem.* **1960**, *64*, 188.
[34] J. M. Artés, I. Díez-Pérez, P. Gorostiza, *Nano Lett.* **2012**, *12*, 2679.
[35] W. Zhang, I. J. Burgess, *J. Electroanal. Chem.* **2012**, *668*, 66.
[36] A. Soudackov, S. Hammes-Schiffer, *J. Chem. Phys.* **2000**, *113*, 2385.
[37] R. Tyburski, T. Liu, S. D. Glover, L. Hammarström, *J. Am. Chem. Soc.* **2021**, *143*, 560.
[38] M. P. Ruiz, A. C. Aragonès, N. Camarero, J. G. Vilhena, M. Ortega, L. A. Zotti, R. Pérez, J. C. Cuevas, P. Gorostiza, I. Díez-Pérez, *J. Am. Chem. Soc.* **2017**, *139*, 15337.
[39] J. M. Artés, M. López-Martínez, I. Díez-Pérez, F. Sanz, P. Gorostiza, *Small* **2014**, *10*, 2537.
[40] T. Clark, J. Heske, T. D. Kühne, *ChemPhysChem* **2019**, *20*, 2461.
[41] C. Tempra, V. C. Chamorro, P. Jungwirth, *J. Phys. Chem. B* **2023**, *127*, 1138.
[42] R. Guzzi, C. Arcangeli, A. R. Bizzarri, *Biophys. Chem.* **1999**, *82*, 9.
[43] A. Yang, M. R. Gunner, R. Sampogna, K. Sharp, B. Honig, *Proteins: Struct., Funct., Bioinf.* **1993**, *15*, 252.
[44] S. C. L. Kamerlin, M. Haranczyk, A. Warshel, *J. Phys. Chem. B* **2009**, *113*, 1253.
[45] A. Warshel, *Biochemistry* **1981**, *20*, 3167.
[46] J. C. Gordon, J. B. Myers, T. Folta, V. Shoja, L. S. Heath, A. Onufriev, *Nucleic Acids Res.* **2005**, *33*, W368.
[47] M. H. M. Olsson, C. R. Søndergaard, M. Rostkowski, J. H. Jensen, *J. Chem. Theory Comput.* **2011**, *7*, 525.
[48] M. Imai, T. Saio, H. Kumeta, T. Uchida, F. Inagaki, K. Ishimori, *Biochem. Biophys. Res. Commun.* **2016**, *469*, 978.
[49] M. H. V. Huynh, T. J. Meyer, *Chem. Rev.* **2007**, *107*, 5004.
[50] S. Hammes-Schiffer, A. V. Soudackov, *J. Phys. Chem. B* **2008**, *112*, 14108.
[51] A. Migliore, N. F. Polizzi, M. J. Therien, D. N. Beratan, *Chem. Rev.* **2014**, *114*, 3381.
[52] S. Y. Reece, J. M. Hodgkiss, J. Stubbe, D. G. Nocera, *Philosoph. Trans. Royal Soc. B: Biol. Sci.* **2006**, *361*, 1351.
[53] J. F. Turrens, *J Physiol* **2003**, *552*, 335.
[54] M. K. Beissenhirtz, F. W. Scheller, F. Lisdat, *Anal. Chem.* **2004**, *76*, 4665.
[55] P. M. Wood, *FEBS Lett.* **1974**, *44*, 22.
[56] B. B. Blizanac, P. N. Ross, N. M. Markovic, *Electrochim. Acta* **2007**, *52*, 2264.
[57] J. Sun, B. L. Trumpower, *Arch. Biochem. Biophys.* **2003**, *419*, 198.
[58] L. Bleier, S. Dröse, *Biochim. Biophys. Acta (BBA) - Bioenergetics* **2013**, *1827*, 1320.
[59] J. Liu, M. Liu, H. Zhang, W. Guo, *Angew. Chem., Int. Ed.* **2021**, *60*, 12992.
[60] A. Guerra-Castellano, A. Díaz-Quintana, B. Moreno-Beltrán, J. López-Prados, P. M. Nieto, W. Meister, J. Staffa, M. Teixeira, P. Hildebrandt, M. A. Dela Rosa, I. Díaz-Moreno, *Chem. – Euro. J.* **2015**, *21*, 15004.
[61] J. L. Olloqui-Sariego, G. Pérez-Mejías, I. Márquez, A. Guerra-Castellano, J. J. Calvente, M. A. De la Rosa, R. Andreu, I. Díaz-Moreno, *Biochim. Biophys. Acta (BBA) - Bioenergetics* **1863**, *2022*, 148570.
[62] G. Pérez-Mejías, J. L. Olloqui-Sariego, A. Guerra-Castellano, A. Díaz-Quintana, J. J. Calvente, R. Andreu, M. A. De la Rosa, I. Díaz-Moreno, *Biochim. Biophys. Acta (BBA) - Bioenergetics* **2020**, *1861*, 148277.
[63] S. Cukierman, *Biochim. Biophys. Acta (BBA) - Bioenergetics* **2006**, *1757*, 876.
[64] R. A. Horne, E. H. Axelrod, *J. Chem. Phys.* **1964**, *40*, 1518.
[65] I. M. Klotz, J. Ayers, J. Y. C. Ho, M. G. Horowitz, R. E. Heiney, *J. Am. Chem. Soc.* **1958**, *80*, 2132.
[66] R. A. Horne, *J. Inorganic Nucl. Chem.* **1963**, *25*, 1139.
[67] V. Vargová, M. Zivanović, V. Dorčák, E. Paleček, V. Ostatná, *Electroanalysis* **2013**, *25*, 2130.
[68] X. Zhang, F. Xie, S. Ma, C. Ma, X. Jiang, Y. Yi, Y. Song, M. Liu, P. Zhao, X. Ma, *Front. Cell Dev. Biol.* **2023**, *11*, 1283820.
[69] R. R. Nazmutdinov, S. A. Shermokhamedov, T. T. Zinkicheva, J. Ulstrup, X. Xiao, *Chem. Soc. Rev.* **2023**, *52*, 6230.
[70] E. Odella, M. Secor, E. A. Reyes Cruz, W. D. Guerra, M. N. Urrutia, P. A. Liddell, T. A. Moore, G. F. Moore, S. Hammes-Schiffer, A. L. Moore, *J. Am. Chem. Soc.* **2022**, *144*, 15672.
[71] Z. Zhou, Z. Chen, X. W. Kang, Y. Zhou, B. Wang, S. Tang, S. Zou, Y. Zhang, Q. Hu, F. Bai, B. Ding, D. Zhong, *Proc. Natl. Acad. Sci. USA* **2022**, *119*, 2203996119.
[72] A. M. Kuznetsov, J. Ulstrup, *Can. J. Chem.* **1999**, *77*, 1085.
[73] J. P. Klinman, A. R. Offenbacher, *Acc. Chem. Res.* **2018**, *51*, 1966.
[74] A. Migliore, S. Corni, R. Di Felice, E. Molinari, *J. Phys. Chem. B* **2007**, *111*, 3774.
[75] S. Keinan, J. M. Nocek, B. M. Hoffman, D. N. Beratan, *Phys. Chem. Chem. Phys.* **2012**, *14*, 13881.
[76] U. Khaniya, C. Gupta, X. Cai, J. Mao, D. Kaur, Y. Zhang, A. Singharoy, M. R. Gunner, *Biochim. Biophys. Acta (BBA) - Bioenergetics* **2020**, *1861*, 148240.
[77] E. T. Judd, N. Stein, A. A. Pacheco, S. J. Elliott, *Biochemistry* **2014**, *53*, 5638.
[78] H. Ishikita, K. Saito, *J. R Soc. Interface* **2014**, *11*, 20130518.
[79] H. N. Raum, K. Modig, M. Akke, U. Weininger, *J. Am. Chem. Soc.* **2024**, *146*, 22284.
[80] B. A. Barry, J. Chen, J. Keough, D. Jenson, A. Offenbacher, C. Pagba, *J. Phys. Chem. Lett.* **2012**, *3*, 543.
[81] J. M. García-Heredia, A. Díaz-Quintana, M. Salzano, M. Orzáez, E. Pérez-Payá, M. Teixeira, M. A. De la Rosa, I. Díaz-Moreno, *JBIC J. Biol. Inorganic Chem.* **2011**, *16*, 1155.
[82] S. H. Speck, S. Ferguson-Miller, N. Osheroff, E. Margoliash, *Proc. Natl. Acad. Sci. USA* **1979**, *76*, 155.
[83] B. Moreno-Beltrán, I. Díaz-Moreno, K. González-Arzola, A. Guerra-Castellano, A. Velázquez-Campoy, M. A. De la Rosa, A. Díaz-Quintana, *FEBS Lett.* **2015**, *589*, 476.
[84] A. P. Lobez, F. Wu, J. M. Di Trani, J. L. Rubinstein, M. Oliveberg, P. Brzezinski, A. Moe, *Nat. Commun.* **2024**, *15*, 8241.
[85] G. Pérez-Mejías, A. Díaz-Quintana, A. Guerra-Castellano, I. Díaz-Moreno, M. A. De la Rosa, *Coord. Chem. Rev.* **2022**, *450*, 214233.
[86] C. Vasilev, J. Nguyen, A. G. M. Bowie, G. E. Mayneord, E. C. Martin, A. Hitchcock, T. V. Pogorelov, A. Singharoy, C. N. Hunter, M. P. Johnson, *J. Am. Chem. Soc.* **2024**, *146*, 20019.
[87] A. Singharoy, A. M. Barragan, S. Thangapandian, E. Tajkhorshid, K. Schulten, *J. Am. Chem. Soc.* **2016**, *138*, 12077.
[88] C. K. Chan, A. Singharoy, E. Tajkhorshid, *Biochemistry* **2022**, *61*, 385.
[89] P. Hildebrandt, M. Stockburger, *Biochemistry* **1989**, *28*, 6710.
[90] D. Huang, A. D. Robison, Y. Liu, P. S. Cremer, *Biosens. Bioelectron.* **2012**, *38*, 74.
[91] W. Bian, W. Wu, B. Wang, W. Tang, M. Zhou, C. Jin, H. Ding, W. Fan, Y. Dong, J. Li, D. Ding, *Nature* **2022**, *604*, 479.
[92] A. R. Variyam, M. Stolov, J. Feng, N. Amdursky, *ACS Nano* **2024**, *18*, 5101.
[93] N. Amdursky, X. Wang, P. Meredith, D. D. C. Bradley, M. M. Stevens, *Adv. Mater.* **2016**, *28*, 2692.

[94] D. D. Ordinario, L. Phan, W. G. Walkup, J.-M. Jocson, E. Karshalev, N. Hüsken, A. A. Gorodetsky, *Nat. Chem.* **2014**, *6*, 596.
[95] L. Luo, S. Manda, Y. Park, B. Demir, J. Sanchez, M. P. Anantram, E. E. Oren, A. Gopinath, M. Rolandi, *Nat. Commun.* **2023**, *14*, 5364.
[96] J. Martínez-Fábregas, I. Díaz-Moreno, K. González-Arzola, S. Janocha, J. A. Navarro, M. Hervás, R. Bernhardt, A. Velázquez-Campoy, A. Díaz-Quintana, M. A. De la Rosa, *Mol. Cellular* **2014**, *13*, 1439.
[97] "DOTABLES," https://water.usgs.gov/water-resources/software/DOTABLES/ (accessed: August 2025).
[98] "The Concentration and Isotopic Fractionation of Gases Dissolved in Freshwater in Equilibrium with the Atmosphere. 1. Oxygen on JSTOR," https://www.jstor.org/stable/2835754, (accessed: August 2025).
[99] M. Price, L. Heilbrun, D. Kessel, *Photochem. Photobiol.* **2013**, *89*, 683.
[100] K. N. Ingenbosch, S. Quint, M. Dyllick-Brenzinger, D. S. Wunschik, J. Kiebist, P. Süss, U. Liebelt, R. Zuhse, U. Menyes, K. Scheibner, C. Mayer, K. Opwis, J. S. Gutmann, K. Hoffmann-Jacobsen, *ChemBioChem* **2021**, *22*, 398.
[101] J. Myers, G. Grothaus, S. Narayanan, A. Onufriev, *Proteins: Struct., Funct., Bioinf.* **2006**, *63*, 928.
[102] "BLAST: Basic Local Alignment Search Tool," https://blast.ncbi.nlm.nih.gov/Blast.cgi (accessed: August 2025).
[103] "Clustal O.<. EMBL-EBI," https://www.ebi.ac.uk/jdispatcher/msa/clustalo (accessed: August 2025).
[104] A. M. Waterhouse, J. B. Procter, D. M. A. Martin, M. Clamp, G. J. Barton, *Bioinformatics* **2009**, *25*, 1189.
[105] "Jalview Home Page - Jalview," https://www.jalview.org/ (accessed: August 2025).